buildings

MDPI

Article

Street Geometry Factors Influencing Outdoor Pedestrian Thermal Comfort in a Historic District

Bin Lai [1,†], Jian-Ming Fu [1,†], Cheng-Kai Guo [2], Dan-Yin Zhang [2] and Zhi-Gang Wu [2,*]

[1] Architecture & Public Transportation Design Institute, Huadong Engineering (Fujian) Corporation Limited, Fuzhou 350003, China; lai_b@hdec.com (B.L.); fu_jm@hdec.com (J.-M.F.)
[2] School of Architecture and Urban–Rural Planning, Fuzhou University, Fuzhou 350108, China; 231527008@fzu.edu.cn (C.-K.G.); 231520030@fzu.edu.cn (D.-Y.Z.)
* Correspondence: klins@fzu.edu.cn
† These authors contributed equally to this work.

Abstract: As China's urbanization progresses, the urban heat island (UHI) effect has become more pronounced, impacting the health of residents and the activity intentions of visitors within historic urban areas. This study focuses on the historic district of the Three Lanes and Seven Alleys Tourist Area (SFQX) in Fuzhou, where simulations were conducted on four representative streets across various times during a typical summer meteorological day. Typological methods were employed to simplify neighborhood modeling, and Phoenics software was utilized to simulate the neighborhood's wind environment and the outdoor pedestrian thermal comfort index. Aspect ratio (AR), sky view factor (SVF), air velocity (Va), and universal thermal climate index (UTCI) values at specific locations were collected for statistical analysis. The findings reveal that: (1) the N–S orientation exhibits more significant correlations between Va, the UTCI, and street geometry compared to the E–W orientation; (2) the relationship between SVF and the UTCI fluctuates with time; (3) areas with higher AR values, such as medium and deep canyons, offer better thermal comfort for outdoor pedestrians; and (4) at 8:00, the UTCI and wind speed show minimal correlations with street geometry and direction, being predominantly influenced by objective climatic factors. These insights are expected to significantly inform the geometric design and planning of streets in Fuzhou's historic districts, aiming to create more comfortable outdoor environments for inhabitants and visitors alike.

Keywords: historic district; street geometry; pedestrian thermal comfort (PTC); aspect ratio (AR); sky view factor (SVF)

check for updates

Academic Editor: Vincenzo Costanzo

Received: 13 December 2024
Revised: 11 January 2025
Accepted: 5 February 2025
Published: 17 February 2025

Citation: Lai, B.; Fu, J.-M.; Guo, C.-K.; Zhang, D.-Y.; Wu, Z.-G. Street Geometry Factors Influencing Outdoor Pedestrian Thermal Comfort in a Historic District. *Buildings* **2025**, *15*, 613. https://doi.org/10.3390/buildings15040613

Copyright: © 2025 by the authors. Licensee MDPI, Basel, Switzerland. This article is an open access article distributed under the terms and conditions of the Creative Commons Attribution (CC BY) license (https://creativecommons.org/licenses/by/4.0/).

1. Introduction

With rapid urbanization and altered urban spatial form, the issue of the urban heat island (UHI) effect has become increasingly prevalent and substantially threatens residents' well-being and community health [1,2]. The UHI effect refers to the higher temperature level in cities than in its surrounding areas [3]. The situation is particularly severe in high-density urban areas with tropical climates [4,5]. Concurrently, this effect modifies the outdoor microclimate at the pedestrian level [6,7]. The most prominent impact is the obstruction of airflow within the city, which affects the wind environment and thermal comfort at the pedestrian level [8,9]. Outdoor pedestrian thermal comfort (PTC) is one of the critical factors directly affecting the perceived quality of urban open space [10]. It impacts people's inclination to participate in outdoor activities [11]. Hence, the thermal comfort of outdoor spaces has garnered considerable attention in sustainable urban design [12].

Moreover, an optimal wind environment in urban areas can enhance human comfort. It aids in eliminating pollutants from urban canyons [13–15]. Favorable wind conditions can also mitigate the negative impact of the UHI effect [6,16,17]. Furthermore, studies foresee that extreme heat events will dramatically increase [18]. Therefore, enhancing the wind environment and outdoor pedestrian thermal comfort at the pedestrian level is paramount.

According to the ASHRAE, PTC is a psychological state of satisfaction with the surrounding thermal environment [19]. PTC is influenced by a range of factors, including physical, physiological, psychological, social, and behavioral factors [20]. Among the physical factors, the primary climate parameters include air temperature (Ta), relative humidity (RH), global radiation (G), and air velocity (Va), which are crucial in affecting PTC [20,21]. Furthermore, spatial characteristics such as the type of underlying surface [22,23], vegetation type [24], sky view factor (SVF), and spatial layout [25] are also integral physical factors influencing PTC.

Research on human thermal comfort has always been addressed. Early studies primarily concentrated on indoor thermal comfort. For example, Mishra and Ramgopal provided a detailed review of indoor thermal comfort over the past few decades [26]. Later, research on outdoor thermal comfort shifted into focus, covering large, medium, and minor scales [27]. Large-scale studies assess the impact of urban morphology on thermal comfort. For instance, Abdallah and Mahmoud explored how urban morphology affects outdoor thermal comfort in hot, arid climates [28]. At the neighborhood scale, studies have examined the impact of the residential environment on comfort. For example, Du analyzed the combined influence of visual, auditory, and thermal perceptions on the comfort of older adults in residential outdoor environments [29]. Building-scale studies are also widely conducted. For instance, Eslamirad proposed a data-driven approach to assess outdoor thermal and wind comfort in northern urban environments [30]. There has been substantial research at the urban street scale. For example, Cárdenas-Jirón measured the impact of street configuration on human thermal comfort [31]. However, direct research on the impact of street geometry on outdoor thermal comfort remains scarce [32], especially in historic districts. Historic districts possess rich cultural heritage, unique socioeconomic characteristics, lifestyles, and historical origins, forming distinctive multifunctional street spaces [33]. Historic districts reflect past public life in both material and cultural aspects, holding high preservation value [27]. Therefore, studying the impact of street geometry on outdoor comfort in historic districts is of vital importance.

This study focuses on the geometric characteristics of streets and alleys in historic districts, explicitly addressing the aspect ratio (AR) and SVF of urban canyons. Urban street canyons refer to areas in cities or towns where streets are flanked by continuous or nearly continuous building lines [34]. These canyons are commonly considered as the basic structural unit of the urban canopy layer [35]. Outdoor thermal comfort in urban street canyons has been extensively studied under various climatic conditions, as it affects environmental air temperature, air quality, human health, and energy use [36]. Among them, most research has focused on temperate and tropical regions, such as the Mediterranean climate in Greece [37,38], Tunisia [39], and Barcelona [40], the subtropical climate in Baghdad [36], and the tropical climate in Southeast Asia [41]. Potchter's review article summarizes thermal comfort studies in different climatic zones around the world [42].

At the same time, the evaluation of outdoor thermal comfort in urban streets is often based on the urban canyon as the evaluation unit [43]. AR [44] and SVF [45] can be used to characterize urban canyons. AR is the ratio of building height (H) to street width. SVF is a geometric quantification of the sky's visibility within the street canyon, which is a commonly used indicator to describe a city's geometric shape and is also an effective indicator for measuring urban thermal comfort [46]. SVF is essential in studying the

relationship between urban street geometry and the urban heat island effect. For example, the research of F. Bourbia and F. Boucheriba showed that SVF and street AR significantly affect the solar radiation received by streets, which in turn impacts the thermal comfort of pedestrians [47]. Research by Nazanin Nasrollahi, Yasaman Namazi, and Mohammad Taleghani indicated that the street orientation and aspect ratio significantly impact street shading, which further affects pedestrian thermal comfort [48]. SVF effectively reflects the geometric shape of streets. Therefore, this study uses the SVF index to evaluate urban streets' shading and thermal comfort. The research employs the universal thermal climate index (UTCI) to describe outdoor thermal comfort. UTCI is one of the most used indices for assessing outdoor thermal comfort [41]. The German Cost Action 730 proposed in 2009 is an index that is internationally recognized as a standard for thermal comfort assessment. UTCI can precisely calculate the thermal stress experienced by the human body using air temperature, relative humidity, wind speed, and mean radiant temperature [27].

The study area is in Fuzhou City, Fujian Province, China. According to data from the National Climate Center (NCC) of China, Fuzhou was the hottest city among Chinese provincial capitals from 1981 to 2010. In addition, the urbanization level of Fuzhou increased from 51.5% in 2000 to 73.3% in 2022, making it the fastest developing city in Southeast China over the past 40 years. The environment and microclimate face significant challenges, with its temperature and urban heat island (UHI) effect being highly representative [49]. The Three Lanes and Seven Alleys Tourist Area (SFQX), a 5A-rated national tourist attraction in Fuzhou, is responsible for hosting many visitors. At the same time, "SFQX" is also an obvious high-temperature zone in the Fuzhou urban area, which has high research value in studying outdoor pedestrian thermal comfort. Over the past decade, several studies have assessed the urban heat island (UHI) effect and street thermal comfort in Fuzhou, but most of these studies focused on a macro perspective, analyzing climate and geographical features. Few studies have focused on the thermal comfort of traditional street districts and street morphology in Fuzhou. For example, the research by Zheng mainly focused on the UHI effect in view of the impact of urbanization and topography on thermal comfort during heatwaves in Fuzhou [50], but the research object was more from a macro perspective and the thermal comfort of specific streets was less involved.

Some studies have explored the impact of spatiotemporal changes in street geometry on pedestrian thermal comfort (PTC). For example, the research by Nicholson suggested that the mobility of urban form and the complexity of street sequences enhance the diversity of thermal sensation and that providing a more detailed description of urban entities is beneficial for studying the relationship between geometry and PTC [51]. The study by Mohite and Surawar indicated that the geometry of urban streets is flexible but complex [52]. Therefore, the increase or decrease in solar radiation caused by changes in street geometry leads to significant changes in street microclimate, which affects the thermal experience of outdoor pedestrian. From the pedestrian's perspective, the geometric parameters of streets in "SFQX" are also dynamically changing, and the microclimate along the streets varies. Therefore, the spatiotemporal changes in street geometry and outdoor pedestrian thermal comfort in historic districts like "SFQX" require further investigation. This study aims to address the following issues: 1. The impact of spatiotemporal changes in street geometry on the wind environment and outdoor pedestrian thermal comfort in historic districts; 2. Suggestions for improving the outdoor thermal environment of historic districts in Fuzhou City in summer.

2. Materials and Methods

This study was divided into five steps (Figure 1). In the first step, "SFQX" in Fuzhou City was selected, depicting the typical characteristics of a historic district. After conduct-

ing a survey and research on the selected district using QGIS (v3.40) software, a physical map was made. This involved creating digital representations of streets, such as buildings, alleys, and other facilities, along with building classification. In the second step, field measurements were carried out on the classified buildings and each street. The purpose was to obtain street geometry parameters such as AR and SVF. Meanwhile, climate data, including Ta, RH, Va, and G, were obtained through meteorological websites. In the third step, the on-site research data and the climate data served as the input data. Phoenics@2019 software was used to simulate the outdoor wind environment and thermal comfort indices, from which the Va and UTCI values were derived. Additionally, Rayman Pro@3.1 software was employed to verify and calculate SVF. In the fourth step, the data collected during the on-site research and the simulation results were used for statistical analysis. The goal was to explore the relationship between the street geometry of the historic district and the pedestrian thermal comfort in the fifth step.

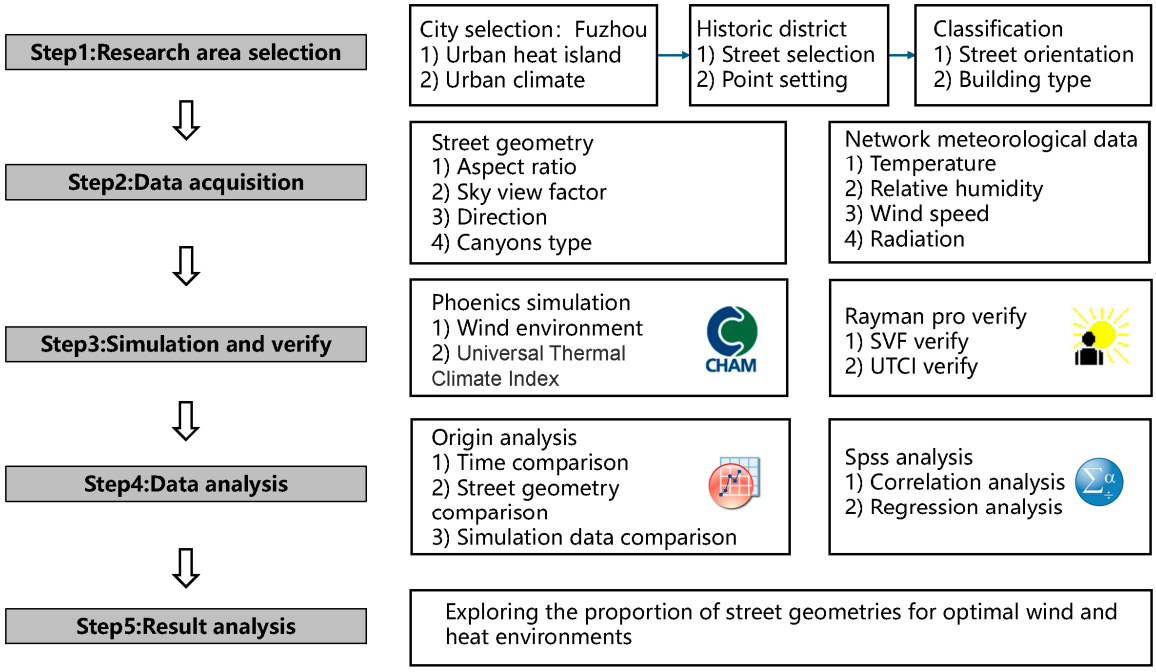


Figure 1. Research methods.

2.1. Overview of the Research Object

This study was conducted in the historic district of "SFQX" in Fuzhou, China, at 26.0809° north latitude and 119.2968° east longitude. According to the classification in the "Standard for Building Climate Zoning" [53] in China, Fuzhou is located in a region with hot summers and warm winters. The annual temperature varies, with a minimum of −2 °C in winter (from December to February) and a maximum of 41 °C in summer (from June to August). Because of Fuzhou's basin terrain, there is a solid UHI effect in the central urban area (CUA) of Fuzhou at present. Urban residents face increasingly high risks of heat cramps, fatigue, fainting, and heatstroke. "SFQX" is a historic and cultural district in China that has a relatively sizeable scale and is well protected. It also has a good reputation as "the living fossil of the urban district system in China" and "the museum of Ming and Qing architecture in China". Previous studies have indicated that the UHI effect occurs in the CUA [50,53,54]. Furthermore, "SFQX" is an obvious high-temperature point in the CUA. Moreover, most buildings in the district are low ancient residential building groups. Therefore, studying the pedestrian thermal comfort in "SFQX" during summer is significant.

2.1.1. Street Selection

QGIS (v3.40) software was used to model the district digitally, reproducing the building types, building heights, and street orientations. Based on the base map drawn and the heat map in Baidu map, this study analyzed the flow of people and selected four representative streets and alleys (NanHou Street, WenRu Alley, AnMing Alley, and MinShan Alley). NanHou (NH) Street, as the central axis of the historic district, is the main commercial street, flanked by shops in the traditional "ChaiLanCuo (CLC)" style, with the widest street in the district and the highest pedestrian flow. By comparison, MinShan (MS) Alley has the same orientation as NH Street but is characterized by narrower alleys and is mainly lined with courtyard-style buildings with gable walls, creating a quieter environment with low pedestrian traffic. WenRu (WR) Alley and AnMing (AM) Alley are linearly distributed and intersect with NH Street, with pedestrian flow second only to NH Street. WR Alley is the most representative among the three alleys. It has a regular layout, distributed with many traditional courtyard dwellings facing the alley. AM Alley, opposite WR Alley, has a narrower average width, but the building form and layout are like those of WR Alley. The four selected streets and alleys cover the geometric conditions of most of the streets in the historic district of "SFQX" in terms of direction, aspect ratio (AR), and sky view factor (SVF).

2.1.2. Point Setting

The street geometry in historic districts will change with the change in pedestrian routes, and the height and width of each section of the streets and alleys are different. Based on the differences in building types on both sides of the streets and alleys and the widths of the streets and alleys, 10 midpoints of typical roads with different aspect ratios were selected on the selected streets and alleys. The geographical locations of the selected streets and alleys in "SFQX" and the specific selection of points are illustrated in Figure 2a.



(**a**)

Figure 2. *Cont.*

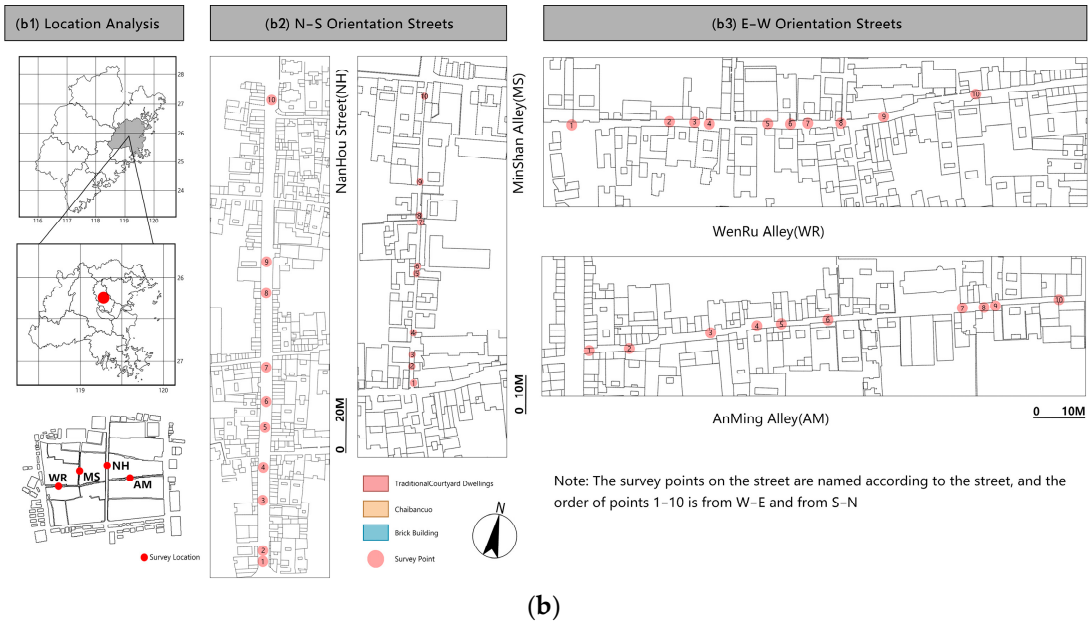


Figure 2. Selection of streets, locations, and building types in "SFQX". (**a**) Street selection and location setup. (**b**) Types of buildings in "SFQX".

2.2. Field Measurement

The physical characteristics of streets (AR, SVF) and typical buildings (H) were collected through field measurements. A Leica D2 handheld red laser rangefinder was employed to measure the heights of buildings and the dimensions of streets and alleys. Before conducting the field measurements outdoors, the instruments were uniformly calibrated and tested. The buildings in "SFQX" are mainly divided into three types: "Chai Lan Cuo", brick buildings, and traditional courtyard dwellings (Figure 2b). "CLC" is a traditional residence in Fuzhou, with a floor height of approximately 2 m and most of them have 2 to 3 floors. They are concentrated in distribution as they are mainly located on both sides of NH Street. The brick buildings in "SFQX", newly constructed in modern times, typically exhibit a floor height of approximately 3.5 m and predominantly comprise 2 to 3 floors. The distribution is uneven, with a higher concentration along NH Street and in the southeast side of the historic district. Traditional courtyard dwellings, which are the most widely distributed historical buildings in "SFQX", are classified as front and side (gable wall surface) based on the orientation of the buildings. The height under the eaves of the front facade (5 m) and the highest point of the side gable wall (6 m) were selected as the typical heights of the traditional courtyard dwellings. Once the heights of standard buildings were selected and measured, a simplified model of the historic district was established, which enabled the design of the heights on both sides of the streets according to the building types.

2.3. Simulation Method

This section focuses on the simulation method, which is the key part of the study for obtaining data and analyzing the impact of street geometry factors on the thermal environment. The chapter describes in detail how to use Phoenics software and the Sky View Analysis plug-in to simulate and accurately set the parameters in the simulation process (see Appendix A for details). At the same time, it introduces methods to verify the accuracy of the simulation results and to ensure the scientific and reliability of the research.

2.3.1. Phoenics Simulation

Phoenics@2019 software was used to conduct simulations to acquire data on the outdoor wind-thermal environment and thermal comfort indices in different time periods.

This software has shown its reliability in research on outdoor thermal comfort [55]. Regarding the simulation time cost and simulation accuracy, this study adopted a horizontal grid resolution of 4 × 4 m, and the vertical grid resolution was set to 4 m. Moreover, the grids on the bottom layer were further subdivided into 3 layers. Vegetation and pavement materials remarkably influence outdoor thermal comfort [56]. However, since this study only focused on discussing the impact of street geometry on PTC in the historic district, the interference caused by plants and pavement materials was excluded. The meteorological data for 22 July, a typical summer meteorological day in Fuzhou, were obtained from the European Centre for Medium-Range Weather Forecasts (ECMWF). Other parameters and attributes are presented in Table 1. Among them, based on the comprehensive consideration of the complex building environment in the region, the high building density of the historic district and the surrounding medium and high-rise buildings were distributed in patches, forming a wide range of obstacles. Therefore, the value of the effective roughness height was set to 0.75 m [57,58]. This research conducted a thorough exploration of street geometry and outdoor pedestrian thermal comfort by relying on simulation technology. By collecting and sorting out other relevant simulation articles, mature modeling ideas, parameter adjustments, and algorithm strategies were drawn on to build a simulation model that met the requirements of this study [59,60]. The comparison and analysis between the simulation results and those of related studies in the existing literature were carried out from multiple dimensions, such as the numerical characteristics, changing trends, and overall data distribution of key indicators, using scientific statistical test methods for detailed comparison, which indirectly provided support for the reliability of the results of this study.

Table 1. Other simulation parameters.

Type	Parameters and Attributes		
Time	8:00	12:00	18:00
Air temperature (°C)	30.7	36.5	29.7
Air humidity (%)	65.8	44.6	70.7
Air pressure (hPa)	977	975	975
Wind direction (°)	56	82	89
Ground wind speed (m/s)	1.25	3	2.8
Surface horizontal radiation (W/m^2)	549	872	38
Normal direct radiation (W/m^2)	508	590	151
Scattered radiation (W/m^2)	216	289	28
Simulated boundary settings	5 times the X-, Y-, and Z-axes of the architectural complex		
Grid settings	The number of grids is 540 × 438 × 52		
Turbulence model	Chen–Kim KE model [61]		
Radiation model	IMMERSOL model [62]		
Profile Type	Power law		
Power law index	0.22		
Effective roughness height	0.75 m [57,58]		
Clothing insulation (clo)	0.5		
Metabolic rate (W/m^2)	90		

Note. Table source: Drawn by the author.

2.3.2. SVF Verify

This study employed the SketchUp plug-in Sky View Analysis (SVA) to calculate SVF. To verify the reliability of the calculation results of the software, root mean square error (RMSE) analysis was carried out on the results by comparing the actual measurements with the simulations. The RMSE is an evaluation indicator widely applied in regression

problems. It measures the average difference between the predicted values and the actual values. The RMSE formula (Equation (1)) is expressed as follows:

$$RMSE = \sqrt{\frac{1}{N}\sum_{i=1}^{N}(y_i - \hat{y}_i)^2} \quad (1)$$

where N stands for the number of samples; y_i represents the SVF value obtained from actual measurement; and $\hat{y}_i$ represents the simulated SVF value.

Measuring points were set at equal distances on the center lines of the selected streets. Photos were taken vertically upward at 1.2 m above the ground with a fisheye lens [63] and then imported into Rayman pro@3.1 software for calculation. The situation concerning the simulated SVF values and the SVF values acquired after on-site measurements is shown in Figure 3. The error calculated with the RMSE formula was 0.121. Since there was interference from tree shade in the actual measurement of SVF, after the points with larger errors were manually excluded, the calculated RMSE was 0.053. Both the RMSE calculated with the method including the error points and the RMSE calculated with the method excluding the points with more significant errors met the experimental design requirements. Therefore, the reliability of the SVA plug-in was verified.

Location	Point 1		Point 2		Point 3		Point 4	
Method	Measure	Simulate	Measure	Simulate	Measure	Simulate	Measure	Simulate
Sky View Factor								
SVF Value	0.752	0.715	0.654	0.735	0.443	0.711	0.682	0.689
Location	Point 5		Point 6		Point 7		Point 8	
Method	Measure	Simulate	Measure	Simulate	Measure	Simulate	Measure	Simulate
Sky View Factor								
SVF Value	0.716	0.7	0.599	0.724	0.542	0.669	0.706	0.784
Legend				Effective Data		Invalid Data		

Figure 3. Simulated and field-measured SVF values.

2.4. Outdoor Thermal Comfort Evaluation Indicators

Outdoor thermal comfort indices generally depend on the human body's heat balance and exchange with the surrounding environment. They are used to assess the thermal comfort of outdoor pedestrians and mainly consist of the following three indices: physiological equivalent temperature (PET), predicted mean vote (PMV), and the UTCI. Among these, the UTCI is a widely adopted human body thermal comfort index based on the theory of physiological heat exchange. The UTCI is a six-degree polynomial equation based on the theory of thermal physiological exchange. It consists of two parts: the Fiala multi node model and adaptive dressing model. The former simulates the process of thermal exchange between the human body and the outside world, while the latter is a correction factor for specific sites [64]. It is more sensitive to the temporal variations of meteorological elements and can reflect the actual situation more effectively than other indices. Since the UTCI applies to different urban scales and climatic conditions, it was selected as the thermal comfort evaluation index in this study [27]. The UTCI in this study was obtained by Phoenics software. The published subroutine returned the UTCI as a function of air temperature, water vapor pressure, average radiation value, temperature, and wind speed 10 m above the ground. In its implementation, the local air temperature was taken as the

simulated temperature, then the local steam pressure was obtained from the simulated steam to obtain the mass fraction, the local average radiation temperature was taken as the simulated radiation temperature, and the local absolute velocity was taken as the wind speed.

The calculation results of the UTCI were divided into 10 levels of comfort, ranging from cold to heat. These levels were used to comprehensively evaluate the thermal comfort of the test site. Specifically, when the UTCI exceeded 46 °C, it represented extreme heat stress. When it was between 38 and 46 °C, it represented very strong heat stress. Between 32 and 38 °C, it indicated strong heat stress. From 26 to 32 °C, it meant moderate heat stress. Between 9 and 26 °C, there was no thermal stress. From 0 to 9 °C, it indicated a slight cold stress. Between −13 and 0 °C, it indicated moderate cold stress. Between −27 and −13 °C, it indicated strong cold stress. Between −40 and −27 °C, it indicated very strong cold stress. Moreover, when the UTCI was lower than −40 °C, it indicated extreme cold stress. The calculation formula of the UTCI is expressed as follows:

$$UTCI = T_a + O_{ffset}(T_a, T_{mrt}, V_a, RH) = f(T_a, T_{mrt}, V_a, RH) \quad (2)$$

where Offset: temperature deviation (°C); Ta: actual temperature (°C); Tmrt: average radiation temperature (°C) (influenced by temperature, relative humidity, air velocity, and black-bulb temperature); Va: air velocity (m/s); RH: relative humidity (%).

2.5. Street Canyon Type

AR, also called the street canyon height-to-width ratio, refers to the ratio between the average height (H) of the buildings on both sides of the street and the width (W) of the street. To study the geometric forms of the streets more clearly, the streets were categorized into three types of street canyons based on the magnitude of the aspect ratio: shallow canyons, medium canyons, and deep canyons (Figure 4).

Type	AR	Characteristic
Shallow canyons	AR < 1	In shallow canyons, the air temperature is usually higher than that in uniform canyons. Especially at noon.
Middle canyons	1≤AR≤2	In such a canyon, the surface temperature is relatively uniform along the length of the canyon. The temperature is relatively uniform.
Deep canyons	AR > 2	The temperature in deep canyons is usually lower than that in uniform canyons, especially during noon hours Deep canyons and their shading effects are suitable for summer, not for winter, and vice versa.

Figure 4. Street canyon classification diagram.

2.6. Spearman's Correlation Analysis

This study used the Spearman correlation coefficient to explore the correlations between street geometry, Va, and the UTCI. It is a non-parametric statistic that measures the strength and direction of the monotonic relationship between two variables [65]. Given that, in this study, the street geometry and the continuous variables did not meet the requirement of normal distribution, the Spearman correlation method in SPSS software was adopted for statistical analysis.

3. Results and Analysis

This section provides a thorough mining and interpretation of the research data to reveal the impact of street geometry on outdoor pedestrian thermal comfort. The relationship between street geometry, Va, and the UTCI is comprehensively presented. The geometric characteristics of the streets of the historic district are described. The research on the temporal and spatial distribution of Va and the UTCI is conducted using a variety of analysis methods, such as data comparison and chart display.

3.1. Historic District Street Geometry

This subsection focuses on the analysis of the geometric shape of the streets in the study area. The N–S streets (such as NH street and MS Alley) and the E–W streets (such as WR Alley and AM Alley) are described respectively, and the key data, such as average width, building height range, AR value, and SVF value, are listed in detail, showing the significant differences in the geometric characteristics of different streets.

3.1.1. North–South-Oriented Streets

When observing the geometric characteristics of the streets shown in Figure 5, it can be noticed that the average widths of NH Street and MS Alley are 11.8 m and 3 m, respectively, showing a significant difference. Nevertheless, these two streets' minimum and maximum building heights are identical, both at 4.5 m and 11 m. NH Street is segmented by multiple east–west streets, having more openings. The buildings on both sides of it are arranged in an orderly manner. The AR values at most positions on NH Street are less than 1. The maximum AR value is 0.79 and the minimum is 0.35, with a relatively small difference. Hence, the street canyon type of NH Street is a uniform shallow canyon. The SVF values range from 0.673 to 0.804. NH6 is the point with the minimum SVF value, while NH9 is the point with the maximum SVF value. MS Alley is narrow, with high buildings on both sides. The overall layout of the buildings is dense, and there are fewer openings. MS Street's AR values range from 0.94 to 3, showing a relatively large overall fluctuation. As a result, the street canyon type of MS Alley is a non-uniform deep canyon. MS10 is the maximum AR value point, and MS1 is the minimum. The SVF values range from 0.191 to 0.508. MS10 is the point with the minimum SVF value, and MS1 is the point with the maximum SVF value.

Location	NH1	NH2	NH3	NH4	NH5	NH6	NH7	NH8	NH9	NH10
Aspect Ratio										
AR Value	0.56	0.48	0.57	0.71	0.7	0.79	0.52	0.65	0.35	0.57
SVF										
SVF Value	0.711	0.747	0.703	0.696	0.71	0.673	0.736	0.675	0.804	0.785
Location	MS1	MS2	MS3	MS4	MS5	MS6	MS7	MS8	MS9	MS10
Aspect Ratio										
AR Value	0.94	2.31	2358	1.88	2.05	1.44	1.16	2	1.9	3
SVF										
SVF Value	0.508	0.246	0.262	0.262	0.289	0.356	0.351	0.291	0.287	0.191

Figure 5. Geometric characteristics of north–south streets.

3.1.2. East–West-Oriented Streets

Upon observing Figure 6, both WR Alley and AM Alley have relatively dense buildings on both sides of the alleys. Moreover, their overall forms and layouts are alike. The average width of WR Alley is 4.8 m, and its minimum building height is 4.5 m. The canyon types of this alley are mainly shallow and medium canyons, yet the distribution is uneven. The AR values of WR Alley range from 0.8 to 2.02. WR7 is where the AR value is at its minimum, while WR5 is where the AR value reaches its maximum. The SVF values of WR Alley range from 0.326 to 0.548. WR5 is the point with the minimum SVF value, and WR4 is the point with the maximum SVF value. The average width of AM Alley is 3.9 m, and its maximum building height is 14.5 m. The canyon types are mainly medium and high canyons, and the distribution is also uneven. In AM Alley, AR is maximized at 2.5 at AM5 and minimized at 0.66 at AM9. The SVF values of AM Alley vary from 0.252 at AM5 to 0.471 at AM9.

Location	WR1	WR2	WR3	WR4	WR5	WR6	WR7	WR8	WR9	WR10
Aspect Ratio										
AR Value	0.91	1.5	1.3	0.83	2.02	1.33	0.8	1.42	0.98	1.76
SVF										
SVF Value	0.52	0.351	0.43	0.548	0.326	0.395	0.514	0.466	0.506	0.421
Location	AM1	AM2	AM3	AM4	AM5	AM6	AM7	AM8	AM9	AM10
Aspect Ratio										
AR Value	1.88	1.64	2.02	1.77	2.5	1.7	1.96	1.65	0.66	1.99
SVF										
SVF Value	0.317	0.354	0.243	0.285	0.252	0.318	0.396	0.41	0.471	0.279

Figure 6. Geometric characteristics of east–west streets.

3.2. The Spatiotemporal Distribution of Va and the UTCI

This subsection discusses the temporal and spatial distribution relationship between street geometry, Va, and the UTCI. In terms of spatial distribution, the differences between N–S and E–W streets are clearly compared through the Va map and the UTCI chart. In terms of time distribution, the overall wind speed time rule is revealed, and the UTCI values of different streets show various characteristics at different times.

3.2.1. The Spatiotemporal Distribution of Va

Figure 7 illustrates the spatiotemporal wind speed distribution on a typical summer climate day within "SFQX". Wind speed, as a factor that influences the evaluation index of outdoor thermal comfort, depends largely on street geometry as well as the relationship between street axes and the dominant wind direction. Regarding the spatial distribution, the average wind speed of streets with a North–South (N–S) orientation is 0.92 m per second, while that of streets with an East–West (E–W) orientation is 1.18 m per second. The wind speed of streets with a N–S orientation is lower than that of streets with an E–W orientation. For streets with a N–S orientation, the wind speed shows a downward trend at the intersections of streets and alleys. For instance, on NH Street, the average wind speed is 0.55 m per second at NH2 and 0.64 m per second at NH7, which are relatively low wind speeds on NH Street. On MS Alley, the average wind speed is 1.04 m per second at MS1 and 0.96 m per second at MS10, which is lower than the wind speed at other positions on MS Alley. Conversely, for streets with an E–W orientation, the wind speed shows an upward trend at the intersections of streets and alleys. On WR Street, WR1 and WR10 have the most significant wind speeds across the street. The same applies to AM Alley. When the street orientation is N–S, the average wind speed of NH Street is 0.72 m per second. The average wind speed of MS Alley is the same as that of AM Alley with an E–W orientation, both being 1.12 m per second and more significant than that of NH Street. Meanwhile, the average wind speed of WR Alley, which also has an E–W orientation, is 1.23 m per second, and its overall wind speed is more significant than that of AM Alley.

In terms of temporal distribution, the overall research indicates that in terms of the average wind speed, the wind speed at 8:00 is the lowest, and the wind speed at 12:00 is the highest (Figure 8). On NH Street, the minimum wind speed occurs at NH4 at 8:00, at 0.3 m per second, and the maximum wind speed occurs at NH5 at 12:00, at 1.61 m per second. The overall wind speed trends on NH Street at 12:00 and 18:00 are the same but opposite to that at 8:00. The wind speed fluctuations at NH2 and NH7 are the smallest throughout the day. On MS Alley, the minimum wind speed appears at MS4 at 12:00, which is 0.56 m per second, and the maximum wind speed occurs at MS5 at 12:00, at 2.25 m per second. The overall wind speed trends on MS Alley at 12:00 and 18:00 are the same, and the wind

speed fluctuations at MS10 are the smallest. On WR Alley, the minimum wind speed is 0.63 m per second at WR7 at 8:00, and the maximum wind speed is 2.64 m per second at WR10 at 12:00. The trends of the wind speed change with time are all the same. On AM Alley, the minimum wind speed is 0.42 m per second at AM9 at 8:00, and the maximum wind speed is 2.64 m per second at WR1 at 12:00. The trends of the wind speed change with time are roughly the same.

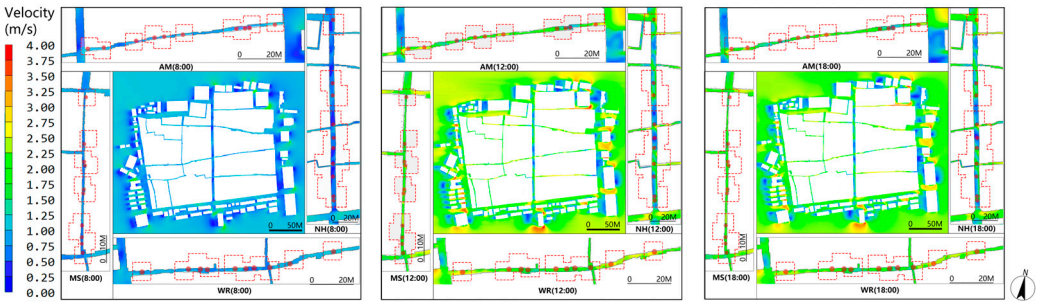


Figure 7. Street wind speed maps for different time periods.

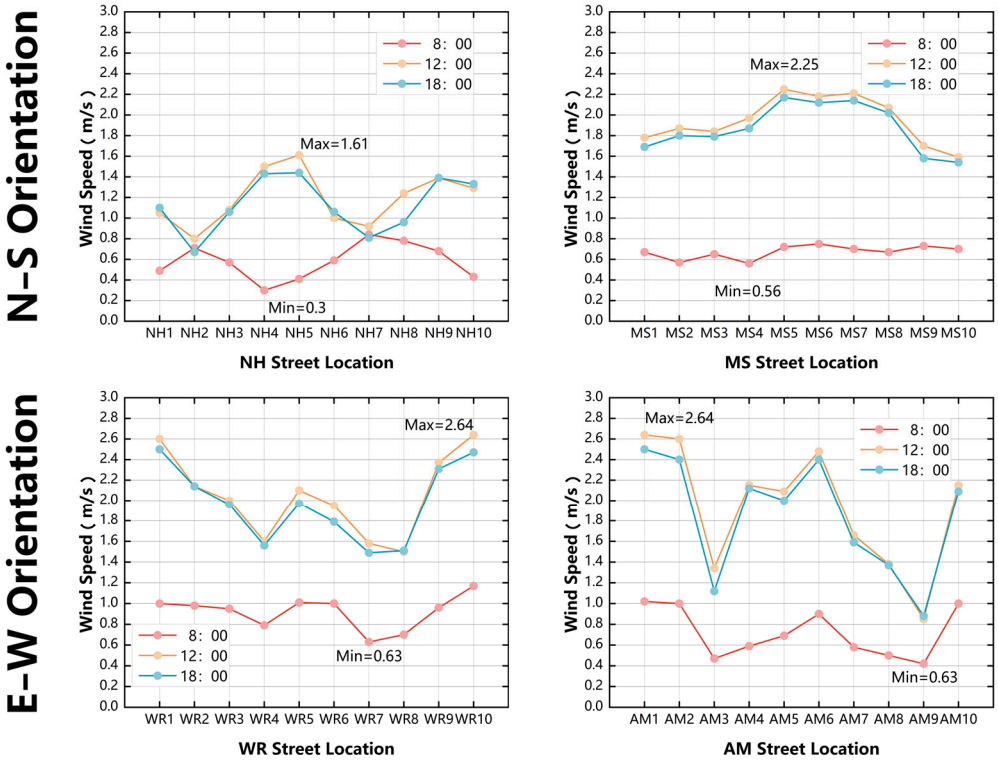


Figure 8. Street wind speed line chart.

3.2.2. The Spatiotemporal Distribution of the UTCI

Figure 9 illustrates the spatiotemporal distribution of the UTCI on a typical climate day in summer within "SFQX". Regarding spatial distribution, the average UTCI of streets with a N–S orientation is 35.75 °C. Compared to streets with an E–W orientation, it is 35.86 °C. Streets with an E–W orientation tend to be hotter than those with a N–S orientation. Among the streets with a N–S orientation, on NH Street, the minimum value of the average UTCI is 35.42 °C at NH9, and the maximum UTCI is 36.63 °C at NH6. On MS Street, the minimum value of the average UTCI is 34.82 °C at MS9, and the maximum value of the average UTCI is 35.66 °C at MS6. Among the streets with an E–W orientation, the average UTCI of WR Street fluctuates between 34.15 °C and 41.54 °C. Specifically, WR1 is where the average UTCI reaches its minimum value, and WR7 is where it reaches its maximum value.

The average UTCI of AM Street varies between 34.62 °C at AM10 and 36.51 °C at AM9. The thermal environment of streets with a N–S orientation is more consistent, while the variation in thermal stress for streets with an E–W orientation is more pronounced. For streets with a N–S orientation, the UTCI values show an upward trend at the intersections of streets and alleys. By contrast, for streets with an E–W orientation, the UTCI values show a downward trend at the intersections of streets and alleys.

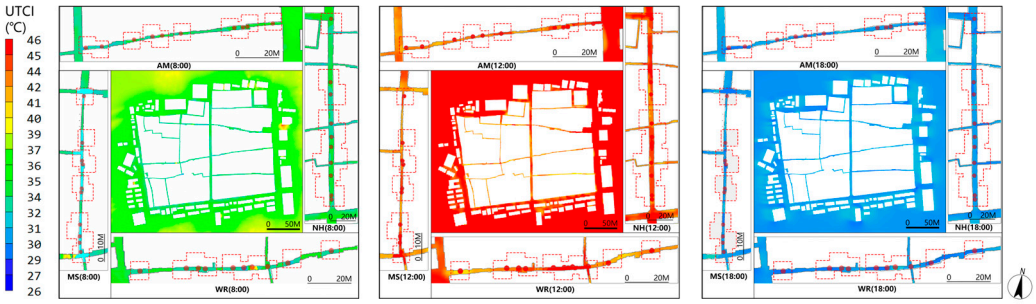


Figure 9. The UTCI graphs for different time periods.

Figure 10 illustrates the temporal variations in the UTCI values in "SFQX". From a macro-level analysis, the outdoor thermal comfort is at its best at 18:00 and at its worst at 12:00. Among the streets with a N–S orientation, the UTCI values of NH Street range from 29.82 °C to 45.76 °C. The maximum value appears at NH6 at 12:00, while the minimum is at NH9 at 18:00. The UTCI values of MS Street range from 29.52 °C to 44.63 °C. The maximum value is found at NH3 at 12:00, and the minimum value is at MS6 at 18:00. Meanwhile, the fluctuation trends of the UTCI curve at noon differ significantly from those in the morning and evening, which suggests that the UTCI values of streets with a N–S orientation are more susceptible to the influence of time. Among the streets with an E–W orientation, the UTCI values of WR Street range from 28.78 °C to 58.56 °C. A relatively significant change in thermal stress occurs at WR7. The maximum UTCI value is located at WR7 at 12:00, and the minimum UTCI value is at WR1 at 18:00. The UTCI values of AM Street range from 29.29 °C to 44.4 °C. The maximum value is located at NH8 at 12:00, and the minimum is at MS1 at 18:00.

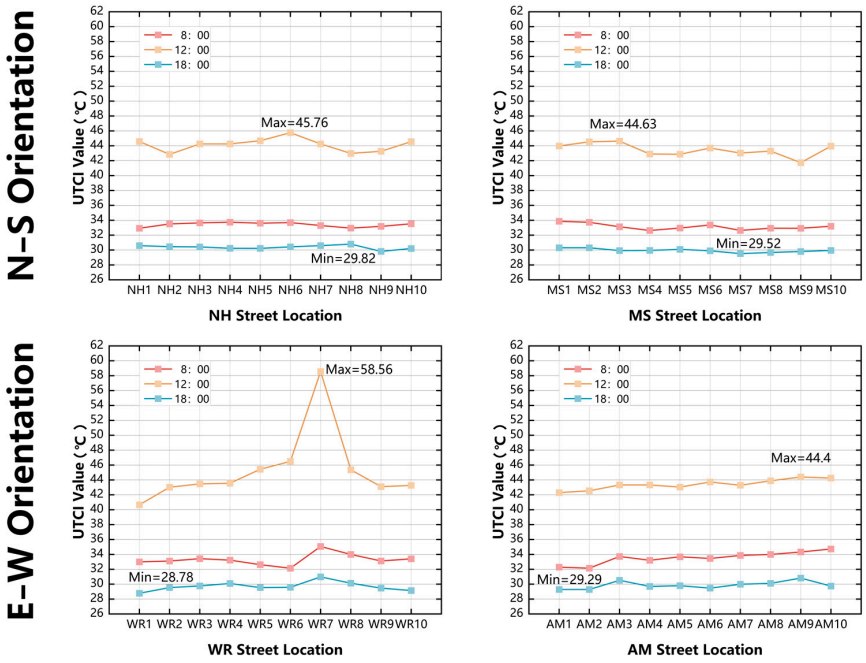


Figure 10. Street UTCI line chart.

3.3. Analysis of the Correlations Between Street Geometry, Va, and UTCI

Table 2 presents the Spearman correlation coefficients between street geometry, Va, and the UTCI during each period and the average period. The results reveal a relatively strong correlation between SVF and Va and a relatively weak correlation between SVF and the UTCI. The correlation between SVF and the UTCI varies over time. The correlation at 18:00 is better than that at 8:00, and there is no correlation at 12:00. The correlation between SVF and Va also changes as time passes and exhibits an increasing trend from morning to night. Meanwhile, it has been discovered that Va of streets with a N–S orientation is more susceptible to the influence of SVF, especially at 18:00 (with a correlation coefficient $r = -0.69$). In addition, in comparison to SVF, Va exhibits a more pronounced correlation with AR. The relationship between AR and Va is influenced by temporal factors, with the most significant correlation observed at 18:00, where the correlation coefficient reaches $r = 0.76$. Based on the above results, the N–S orientation demonstrates stronger correlations between street geometry, Va, and the UTCI than the E–W orientation.

Table 2. Analysis of the correlations between street geometry, Va, and UTCI.

Site	8:00		12:00		18:00		Average Time	
	Va	UTCI	Va	UTCI	Va	UTCI	Va	UTCI
Overall SVF	−0.498 **	0.378 *	−0.514 **	0.201	−0.520 **	0.416 **	−0.498 **	0.378 *
N–S Orientation SVF	−0.119	0.254	−0.67 **	0.179	−0.691 **	0.424	−0.687 **	0.272
E–W Orientation SVF	−0.040	0.077	−0.178	0.141	−0.157	0.205	−0.109	0.274
Overall AR	0.180	−0.122	0.535 **	−0.155	0.541 **	−0.442 **	0.529 **	−0.331 *
N–S Orientation AR	0.057	−0.171	0.739 **	−0.780	0.756 **	−0.507 *	0.747 **	−0.203
E–W Orientation AR	0.110	−0.026	0.205	−0.184	0.171	−0.234	0.150	−0.259

Note. Table source: Drawn by the author; * represents $p < 0.05$ and ** represents $p < 0.01$.

4. Discussion

Observing the overall results of the streets, it can be found that AR, SVF, and street orientation can significantly affect outdoor pedestrian thermal comfort. This conclusion aligns with prior research [32,66]. For instance, Abdollahzadeh and Biloria [65] assessed the outdoor thermal performance of streets in residential areas in Liverpool, Australia and identified street canyon orientation as the most influential factor, accounting for 46.42%, followed by aspect ratio, accounting for 30.59%. In this study, variations in these parameters had a noticeable impact on pedestrian perceptions of the wind-thermal environment across three daily periods. The findings also reveal that, during summer, outdoor pedestrian thermal comfort in the historical district typically exceeds 28 °C. According to UTCI classifications [67], this corresponds to "moderate heat stress" or higher. At the same time, different street canyon types also result in distinct perceptions of the wind-thermal environment among pedestrians (see Figure 11).

AR and SVF are critical indicators for describing street canyon types and exhibit a strong negative correlation. By observing the outdoor pedestrian thermal comfort in different canyon types for both north–south and east–west streets (Figure 12), it can be found that:

(1) In north–south-oriented streets, compared with medium and deep canyons, low canyons have relatively lower AR values and higher SVF values. At 8:00, the UTCI differences are not pronounced, and all three canyon types show similar results. This could be attributed to the lower solar radiation angle in the morning, larger shaded areas, and relatively more comfortable thermal sensation [32]. At 12:00, the UTCI values for low canyons are significantly higher than those of medium and deep canyons. In Fuzhou, a city with a subtropical monsoon climate, low canyons at noon in summer present extreme heat stress, which causes great trouble to the comfort of

pedestrians. This is mainly because the smaller AR values of the low canyons make the solar radiation angle in the street larger, resulting in a larger refracted radiation area in the street alley [48]. Previous studies showed that pedestrians' emotions can affect how they feel heat [68]. In low canyons, strong thermal radiation makes pedestrians feel down, and this negative emotion may worsen the human thermal stress level, which is shown as stronger thermal discomfort by the UTCI. At 18:00, the UTCI values for all three street canyon types remain within the moderate heat stress level, with minor fluctuations generally within a range of 1 [69]. The wind speeds of three street canyons at different time periods show certain regularities. The wind speed at 8:00 is generally lower and more stable than that at noon and in the evening. Compared with the medium and deep canyons, low canyon streets exhibit lower wind speeds at all three time periods. This may be because the AR values of low canyons are relatively small, making it difficult for the streets to form the cold lane effect. As a result, the air velocity is relatively low.

(2) In east–west-oriented streets, the UTCI variations at 8:00 are minimal, suggesting that street canyons have a limited effect on the outdoor thermal comfort of pedestrians in the morning. At 12:00, however, the UTCI values for low canyons show significant fluctuations, ranging from 40.66 to 58.56. This variation may be linked to AR values. The highest UTCI value corresponds to a location with a relatively low AR value, allowing more direct sunlight to reach the ground and raising the temperature. By contrast, the lowest value is associated with a location where the AR value is higher. Narrower streets and denser buildings at this location may promote airflow, helping to dissipate heat and reduce the UTCI values. At 18:00, the UTCI values, consistent with those observed in north–south streets, fall entirely within the moderate heat stress category, exhibiting minimal fluctuations within a narrow range of approximately 1. Similarly, the wind speed patterns align with those of north–south streets. Morning wind speeds are generally lower than those at noon and in the evening. A notable exception occurs at the AM9 location, which is classified as a low canyon. Unlike other low canyon points, this site lies at the intersection of medium and low canyon street types. At this corner, airflow direction may be disrupted by buildings or obstacles, generating turbulence or vortex effects. This causes flow separation and a sharp decline in wind speed.

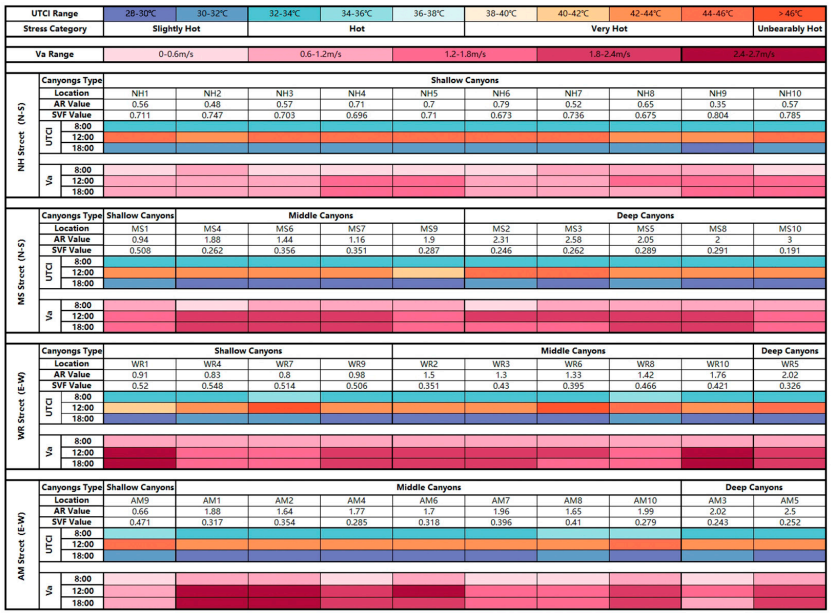


Figure 11. Full indicator calendar chart.

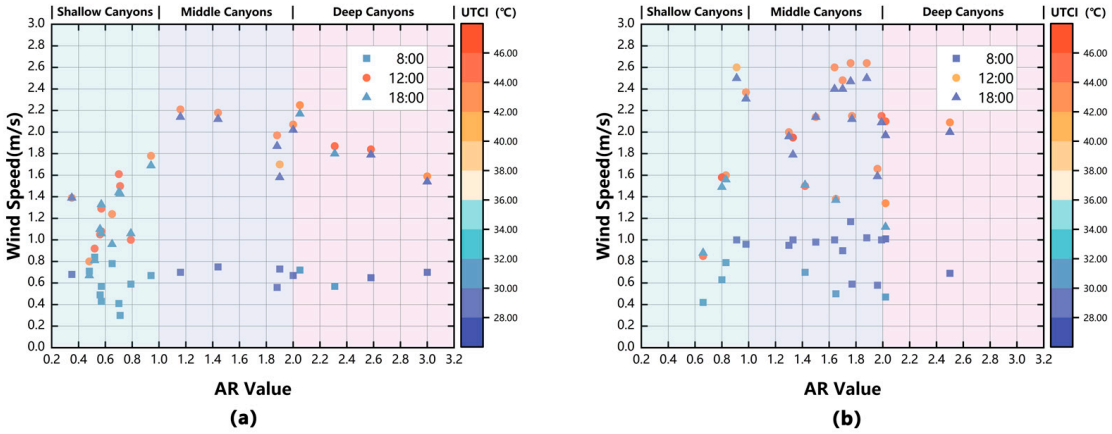


Figure 12. Scatter plot of all indicators. (**a**) N–S Orientation. (**b**) E–W Orientation.

Overall, higher AR values (i.e., medium and deep canyons) performed better regarding outdoor pedestrian thermal comfort. This finding is consistent with the conclusions of Sözen and Oral [44], whose study was also conducted in a hot climatic region. The results, however, vary across different climatic zones. For instance, Sun studied the impact of street geometry on outdoor thermal comfort in cold regions of China [56]. The conclusions they reached are contrary to those of this study. Their research suggested that low and medium canyons ($0.5 < H/W < 1.5$) are more advantageous in severe cold climates. This discrepancy is primarily due to the lower ambient temperatures in cold regions, where the need for heating is far greater than that in hot areas. Under the same solar altitude angle, sunlight can more easily reach the bottom or both sides of low and medium canyon streets, enhancing outdoor pedestrian comfort. Additionally, this study found that the UTCI and wind speed at 8:00 and 18:00 exhibited weaker correlations with street geometry and orientation. It was mainly determined by objective climatic parameters corresponding to these two time periods. In the morning, the atmospheric boundary layer is just beginning to develop, with a relatively low height, leading to weaker vertical and horizontal air movement. Limited momentum transfer restricts near-surface wind speeds, resulting in lower wind velocities. At dusk, as heat dissipates gradually, these dynamic thermal changes further diminish the short-term influence of street geometry and orientation on thermal comfort. By contrast, at 12:00, the UTCI values of east–west-oriented streets with low aspect ratio (AR) values exhibited more pronounced fluctuations than those of north–south-oriented streets. This indicates that the interaction between the solar radiation angle and the street orientation is significant. Therefore, when implementing urban planning policies to address the low AR values of east–west streets, the unique requirements of preserving the character of historic and cultural districts need to be taken into account. Urban design interventions can include adding continuous shading structures, implementing vertical greening (such as wall vegetation), or creating green corridors [70,71]. These measures aim to mitigate the negative impact of heat accumulation caused by direct sunlight on the thermal comfort of pedestrians [72–74]. For north–south streets, adjustable wind corridor designs could be implemented to prevent the stagnation of hot air. Additionally, a well-considered arrangement of shrubs and ground cover plants in medium and high AR canyons could balance openness with vegetation coverage, further enhancing thermal comfort. In addition, when assessing outdoor pedestrian thermal comfort, it is essential to consider wind speed separately for coastal regions. This finding aligns with related research. Abdollahzadeh and Biloria [65] identified wind speed as the most influential meteorological parameter affecting outdoor thermal comfort in coastal areas, which often experience strong airflows.

The conclusions drawn from this study hold reference value for other cities with varying climates, cultures, or architectural characteristics. Our research focuses primarily

on historic districts in hot climates, and the findings are largely consistent with existing studies on pedestrian thermal comfort in hot regions, while differing from conclusions drawn in cold regions. This provides valuable insights for creating and optimizing comfort in historic urban districts across different climates on a broad scale. For instance, the "SFQX" district in Fuzhou, as a historic district with unique cultural and architectural characteristics, requires further adjustments to apply these conclusions to cities with different cultural backgrounds. This is mainly due to the need for detailed consideration of regional climatic features and the appropriate application of different building materials. Nonetheless, the finding that street geometry significantly influences pedestrian thermal comfort remains a valuable reference for future assessments or optimizations of thermal comfort in other historic districts. Furthermore, it is essential to establish mechanisms for monitoring and evaluating thermal comfort in historic districts during urban design or urban renewal processes. This would enable regular assessments of street thermal comfort to effectively guide improvements.

There are some limitations in our study. First, the simulation did not use monitoring data for calibration, which may affect the accuracy of the results. Second, the study is limited to the impact of street geometric elements (orientation, AR, SVF) on outdoor pedestrian thermal comfort, excluding the impact of vegetation, pavement materials, and other elements, which may reduce the applicability of the conclusion. In addition, some scholars have paid attention to pedestrians' perception of thermal comfort. For example, Chinazzo and others have proposed that the visual quality of the environment and visual perception will psychologically affect people's thermal perception [75]. Turhan et al. also found that emotional state is one of the important psychological parameters affecting pedestrian thermal sensation [76–78]. Since this study only carried out simulation research on the physiological thermal comfort indicators of people, it may not be able to pay attention to the impact of psychological behavior on pedestrian thermal comfort. In the future, the comparative analysis of actual measurement and simulation data will be improved, considering the psychological perception dimension of pedestrians.

5. Conclusions

As urbanization in China advances, the urban heat island effect (UHI) has become more severe [69]. The urban thermal environment significantly affects the health and well-being of residents, and the thermal comfort of public spaces plays a crucial role in determining residents' engagement in outdoor activities [79]. Considering this, our research is directed toward understanding these impacts. The focus of our study is Fuzhou, a city in China with a subtropical monsoon climate marked by hot summers and mild winters. The CUA of Fuzhou is currently grappling with a pronounced UHI effect. "SFQX", a nationally renowned 5A-level scenic spot in Fuzhou, is frequented by many tourists and is also recognized as one of the city's hotter regions, making it an ideal location for examining outdoor pedestrian thermal comfort. Consequently, investigating the effects of street geometry in the historic "SFQX" district on the thermal comfort of pedestrians is of paramount importance.

This research delves into the influence of street geometry within the historic district of Fuzhou, China on the thermal comfort of pedestrians in outdoor settings. We selected four distinct streets for simulation across three distinct time slots on a summer day. These streets were chosen for their variations in orientation, AR, and SVF. Va and UTCI maps were generated employing Phoenics software to evaluate the thermal comfort of outdoor pedestrians. Concurrently, we collected and statistically analyzed AR, SVF, Va, and UTCI data at specific locations. The findings reveal the following: (1) streets with a N–S orientation demonstrate a more pronounced relationship between street geometry and Va/UTCI

than those with an E–W orientation; (2) the correlation between SVF and UTCI fluctuates with time; (3) areas with higher AR values, indicative of medium and deep canyons, offer enhanced thermal comfort of outdoor pedestrians; and (4) at 8:00, the UTCI and wind speed exhibit diminished correlations with street geometry and direction, being predominantly shaped by climatic factors. These insights are poised to offer significant guidance for the geometric design and planning of streets in Fuzhou's historic districts, aiming to foster more congenial outdoor environments.

Author Contributions: Conceptualization, B.L.; Methodology, J.-M.F.; Software, C.-K.G.; Formal Analysis, Z.-G.W.; Investigation, B.L. and J.-M.F.; Data Curation, C.-K.G.; Writing—Original Draft Preparation, C.-K.G. and D.-Y.Z.; Writing—Review & Editing, B.L.; Supervision, D.-Y.Z. and Z.-G.W. All authors have read and agreed to the published version of the manuscript.

Funding: This research was supported by the Science and Technology Project of Huadong Engineering (Fujian) Corporation Limited (ZKY2021-FJ-02-04).

Data Availability Statement: The data presented in this study are available upon request from the corresponding author due to privacy restrictions.

Conflicts of Interest: Authors Bin Lai and Jian-Ming Fu were employed by the Architecture & Public Transportation Design Institute, Huadong Engineering (Fujian) Corporation Limited. The remaining authors declare that the research was conducted in the absence of any commercial or financial relationships that could be construed as a potential conflict of interest.

Abbreviations

UHI (Urban Heat Island); PTC (Pedestrian Thermal Comfort); Ta (Air Temperature); RH (Relative Humidity); G (Global radiation); Va (Air Velocity); SVF (Sky View Factor); AR (Aspect Ratio); H (Height); UTCI (Universal Thermal Climate Index); NCC (National Climate Center); SFQX (Three Lanes and Seven Alleys Tourist Area); PTC (Pedestrian Thermal Comfort); CUA (Central Urban Area); NH (Nan Hou Street); CLC (Chai Lan Cuo); MS (Min Shan Alley); WR (Wen Ru Alley); AM (An Ming Alley); ECMWF (European Centre for Medium-Range Weather Forecasts); SVA (Sky View Analysis); RMSE (Root Mean Square Error); PET (Physiological Equivalent Temperature); PMV (Predicted Mean Vote); W (Width); N–S (North–South); E–W (East–West).

Appendix A. Input Data Attributes and Output Data Sources

Table A1. Input data attributes and output data sources.

Input Data Type	Parameters and Attributes		
Time	8:00	12:00	18:00
Air temperature (°C)	30.7	36.5	29.7
Air humidity (%)	65.8	44.6	70.7
Air pressure (hPa)	977	975	975
Wind direction (°)	56	82	89
Ground wind speed (m/s)	1.25	3	2.8
Surface horizontal radiation (W/m^2)	549	872	38
Normal direct radiation (W/m^2)	508	590	151
Scattered radiation (W/m^2)	216	289	28
Simulate boundary settings	5 times the X-, Y-, and Z-axes of the architectural complex		
Grid settings	The number of grids is 540 × 438 × 52		
Turbulence model	Chen–Kim KE model [60]		
Radiation model	IMMERSOL model [61]		
Profile Type	Power law		
Power law index	0.22		
Effective roughness height	0.75 m [56,57]		
Clothing insulation (clo)	0.5		
Metabolic rate (W/m^2)	90		

Table A1. *Cont.*

Input Data Type	Parameters and Attributes
Output Data Type	Data Source
AR Value	Field measurement
SVF Value	Rayman pro@3.1 software
Va Value	PHOENICS@2019 software
UTCI Value	PHOENICS@2019 software
Correlation Value	SPSS@27.0 software

References

1. Akbari, H.; Cartalis, C.; Kolokotsa, D.; Muscio, A.; Pisello, A.L.; Rossi, F.; Santamouris, M.; Synnefa, A.; Wong, H.N.; Zinzi, M. Local climate change and urban heat island mitigation techniques the state of the art. *J. Civ. Eng. Manag.* **2016**, *22*, 1–16. [CrossRef]
2. Behzad, Z.; Guilandoust, A. Enhancing outdoor thermal comfort in a historic site in a hot dry climate (Case study: Naghsh-e-Jahan Square, Isfahan). *Sustain. Cities Soc.* **2024**, *102*, 105209. [CrossRef]
3. Piselli, C.; Castaldo, V.L.; Pigliautile, I.; Pisello, A.L.; Cotana, F. Outdoor comfort conditions in urban areas: On citizens' perspective about microclimate mitigation of urban transit areas. *Sustain. Cities Soc.* **2018**, *39*, 16–36. [CrossRef]
4. Chatzidimitriou, A.; Yannas, S. Microclimate design for open spaces: Ranking urban design effects on pedestrian thermal comfort in summer. *Sustain. Cities Soc.* **2016**, *26*, 27–47. [CrossRef]
5. Elnabawi, M.H.; Hamza, N.; Dudek, S. Thermal perception of outdoor urban spaces in the hot arid region of Cairo, Egypt. *Sustain. Cities Soc.* **2016**, *22*, 136–145. [CrossRef]
6. Du, Y.; Mak, C.M.; Huang, T.; Niu, J. Towards an integrated method to assess effects of lift-up design on outdoor thermal comfort in Hong Kong. *Build. Environ.* **2017**, *125*, 261–272. [CrossRef]
7. Ng, E. Policies and technical guidelines for urban planning of high-density cities–air ventilation assessment (AVA) of Hong Kong. *Build. Environ.* **2009**, *44*, 1478–1488. [CrossRef]
8. Blocken, B.; Carmeliet, J. Pedestrian wind environment around buildings: Literature review and practical examples. *J. Therm. Envel. Build. Sci.* **2004**, *28*, 107–159. [CrossRef]
9. Niu, J.; Liu, J.; Lee, T.C.; Lin, Z.J.; Mak, C.; Tse, K.T.; Tang, B.S.; Kwok, K.C. A new method to assess spatial variations of outdoor thermal comfort: Onsite monitoring results and implications for precinct planning. *Build. Environ.* **2015**, *91*, 263–270. [CrossRef]
10. Zhao, Q.; Sailor, D.J.; Wentz, E.A. Impact of tree locations and arrangements on outdoor microclimates and human thermal comfort in an urban residential environment. *Urban For. Urban Green.* **2018**, *32*, 81–91. [CrossRef]
11. Lai, D.; Zhou, C.; Huang, J.; Jiang, Y.; Long, Z.; Chen, Q. Outdoor space quality: A field study in an urban residential community in central China. *Energy Build.* **2014**, *68*, 713–720. [CrossRef]
12. Banerjee, S.; Yik, S.K.; Dzyuban, Y.; Crank, P.J.; Yi, R.P.X.; Chow, W.T. Analysing impacts of urban morphological variables and density on outdoor microclimate for tropical cities: A review and a framework proposal for future research directions. *Build. Environ.* **2022**, *225*, 109646. [CrossRef]
13. Ai, Z.T.; Mak, C.M. From street canyon microclimate to indoor environmental quality in naturally ventilated urban buildings: Issues and possibilities for improvement. *Build. Environ.* **2015**, *94*, 489–503. [CrossRef] [PubMed]
14. Cui, D.J.; Mak, C.M.; Ai, Z.T.; Kwok, K.C.; Meng, X.Z.; Niu, J.L. On-site evaluation of pedestrian-level air quality at a U-type street canyon in an ancient city. *J. Wind. Eng. Ind. Aerodyn.* **2017**, *168*, 322–333. [CrossRef]
15. Hang, J.; Li, Y. Ventilation strategy and air change rates in idealized high-rise compact urban areas. *Build. Environ.* **2010**, *45*, 2754–2767. [CrossRef]
16. Ignatius, M.; Wong, N.H.; Jusuf, S.K. Urban microclimate analysis with consideration of local ambient temperature, external heat gain, urban ventilation, and outdoor thermal comfort in the tropics. *Sustain. Cities Soc.* **2015**, *19*, 121–135. [CrossRef]
17. O'Malley, C.; Piroozfar, P.; Farr, E.R.; Pomponi, F. Urban Heat Island (UHI) mitigating strategies: A case-based comparative analysis. *Sustain. Cities Soc.* **2015**, *19*, 222–235. [CrossRef]
18. Lee, T.C.; Chan, K.Y.; Ginn, W.L. Projection of extreme temperatures in Hong Kong in the 21st century. *Acta Meteorol. Sin.* **2011**, *25*, 1–20. [CrossRef]
19. Frontczak, M.; Wargocki, P. Literature survey on how different factors influence human comfort in indoor environments. *Build. Environ.* **2011**, *46*, 922–937. [CrossRef]
20. Chen, L.; Ng, E. Outdoor thermal comfort and outdoor activities: A review of research in the past decade. *Cities* **2012**, *29*, 118–125. [CrossRef]
21. Liu, F.; Kang, J. A grounded theory approach to the subjective understanding of urban soundscape in Sheffield. *Cities* **2016**, *50*, 28–39. [CrossRef]

22. Falasca, S.; Ciancio, V.; Salata, F.; Golasi, I.; Rosso, F.; Curci, G. High albedo materials to counteract heat waves in cities: An assessment of meteorology, buildings energy needs and pedestrian thermal comfort. *Build. Environ.* **2019**, *163*, 106242. [CrossRef]
23. Aboelata, A. Reducing outdoor air temperature, improving thermal comfort, and saving buildings' cooling energy demand in arid cities—Cool paving utilization. *Sustain. Cities Soc.* **2021**, *68*, 102762. [CrossRef]
24. Hami, A.; Abdi, B.; Zarehaghi, D.; Maulan, S.B. Assessing the thermal comfort effects of green spaces: A systematic review of methods, parameters, and plants' attributes. *Sustain. Cities Soc.* **2019**, *49*, 101634. [CrossRef]
25. Speak, A.F.; Salbitano, F. Summer thermal comfort of pedestrians in diverse urban settings: A mobile study. *Build. Environ.* **2022**, *208*, 108600. [CrossRef]
26. Mishra, A.K.; Ramgopal, M. Field studies on human thermal comfort—An overview. *Build. Environ.* **2013**, *64*, 94–106. [CrossRef]
27. Li, N.; Guo, Z.; Geng, W.; Li, L.; Li, Z. Design strategies for renovation of public space in Beijing's traditional communities based on measured microclimate and thermal comfort. *Sustain. Cities Soc.* **2023**, *99*, 104927. [CrossRef]
28. Abdallah, A.S.H.; Mahmoud, R.M.A. Urban morphology as an adaptation strategy to improve outdoor thermal comfort in urban residential community of new assiut city, Egypt. *Sustain. Cities Soc.* **2022**, *78*, 103648. [CrossRef]
29. Du, M.; Hong, B.; Gu, C.; Li, Y.; Wang, Y. Multiple effects of visual-acoustic-thermal perceptions on the overall comfort of elderly adults in residential outdoor environments. *Energy Build.* **2023**, *283*, 112813. [CrossRef]
30. Eslamirad, N.; De Luca, F.; Lylykangas, K.S.; Yahia, S.B. Data generative machine learning model for the assessment of outdoor thermal and wind comfort in a northern urban environment. *Front. Archit. Res.* **2023**, *12*, 541–555. [CrossRef]
31. Cárdenas-Jirón, L.A.; Graw, K.; Gangwisch, M.; Matzarakis, A. Influence of street configuration on human thermal comfort and benefits for climate-sensitive urban planning in Santiago de Chile. *Urban Clim.* **2023**, *47*, 101361. [CrossRef]
32. Ali-Toudert, F.; Mayer, H. Numerical study on the effects of aspect ratio and orientation of an urban street canyon on outdoor thermal comfort in hot and dry climate. *Build. Environ.* **2006**, *41*, 94–108. [CrossRef]
33. Lu, L.; Chi, C.G.; Liu, Y. Authenticity, involvement, and image: Evaluating tourist experiences at historic districts. *Tour. Manag.* **2015**, *50*, 85–96. [CrossRef]
34. Pancholy, P.P.; Clemens, K.; Geoghegan, P.; Jermy, M.; Moyers-Gonzalez, M.; Wilson, P.L. Numerical study of flow structure and pedestrian-level wind comfort inside urban street canyons. *J. R. Soc. N. Z.* **2021**, *51*, 307–332. [CrossRef]
35. Ali-Toudert, F.; Mayer, H. Thermal comfort in an east–west oriented street canyon in Freiburg (Germany) under hot summer conditions. *Theor. Appl. Climatol.* **2007**, *87*, 223–237. [CrossRef]
36. Alobaydi, D.; Bakarman, M.A.; Obeidat, B. The impact of urban form configuration on the urban heat island: The case study of Baghdad, Iraq. *Procedia Eng.* **2016**, *145*, 820–827. [CrossRef]
37. Andreou, E. Thermal comfort in outdoor spaces and urban canyon microclimate. *Renew. Energy* **2013**, *55*, 182–188. [CrossRef]
38. Chatzidimitriou, A.; Yannas, S. Street canyon design and improvement potential for urban open spaces; the influence of canyon aspect ratio and orientation on microclimate and outdoor comfort. *Sustain. Cities Soc.* **2017**, *33*, 85–101. [CrossRef]
39. Achour-Younsi, S.; Kharrat, F. Outdoor thermal comfort: Impact of the geometry of an urban street canyon in a Mediterranean subtropical climate–case study Tunis, Tunisia. *Procedia-Soc. Behav. Sci.* **2016**, *216*, 689–700. [CrossRef]
40. Rodríguez Algeciras, J.A.; Matzarakis, A. Quantification of thermal bioclimate for the management of urban design in Mediterranean climate of Barcelona, Spain. *Int. J. Biometeorol.* **2016**, *60*, 1261–1270. [CrossRef] [PubMed]
41. Li, J.; Liu, N. The perception, optimization strategies and prospects of outdoor thermal comfort in China: A review. *Build. Environ.* **2020**, *170*, 106614. [CrossRef]
42. Potchter, O.; Cohen, P.; Lin, T.P.; Matzarakis, A. Outdoor human thermal perception in various climates: A comprehensive review of approaches, methods and quantification. *Sci. Total Environ.* **2018**, *631*, 390–406. [CrossRef] [PubMed]
43. Sözen, İ.; Oral, G.K. Outdoor thermal comfort in urban canyon and courtyard in hot arid climate: A parametric study based on the vernacular settlement of Mardin. *Sustain. Cities Soc.* **2019**, *48*, 101398. [CrossRef]
44. Venhari, A.A.; Tenpierik, M.; Taleghani, M. The role of sky view factor and urban street greenery in human thermal comfort and heat stress in a desert climate. *J. Arid. Environ.* **2019**, *166*, 68–76. [CrossRef]
45. Lin, T.P.; Tsai, K.T.; Hwang, R.L.; Matzarakis, A. Quantification of the effect of thermal indices and sky view factor on park attendance. *Landsc. Urban Plan.* **2012**, *107*, 137–146. [CrossRef]
46. Zhang, J.; Gou, Z.; Lu, Y.; Lin, P. The impact of sky view factor on thermal environments in urban parks in a subtropical coastal city of Australia. *Urban For. Urban Green.* **2019**, *44*, 126422. [CrossRef]
47. Bourbia, F.; Boucheriba, F. Impact of street design on urban microclimate for semi arid climate (Constantine). *Renew. Energy* **2010**, *35*, 343–347. [CrossRef]
48. Nasrollahi, N.; Namazi, Y.; Taleghani, M. The effect of urban shading and canyon geometry on outdoor thermal comfort in hot climates: A case study of Ahvaz, Iran. *Sustain. Cities Soc.* **2021**, *65*, 102638. [CrossRef]
49. Lin, Z.; Xu, H.; Yao, X.; Yang, C.; Yang, L. Exploring the relationship between thermal environmental factors and land surface temperature of a "furnace city" based on local climate zones. *Build. Environ.* **2023**, *243*, 110732. [CrossRef]

50. Zheng, Z.; Lin, X.; Chen, L.; Yan, C.; Sun, T. Effects of urbanization and topography on thermal comfort during a heat wave event: A case study of Fuzhou, China. *Sustain. Cities Soc.* **2024**, *102*, 105233. [CrossRef]
51. Nicholson, S.; Nikolopoulou, M.; Watkins, R.; Löve, M.; Ratti, C. Data driven design for urban street shading: Validation and application of ladybug tools as a design tool for outdoor thermal comfort. *Urban Clim.* **2024**, *56*, 102041. [CrossRef]
52. Mohite, S.; Surawar, M. Impact of urban street geometry on outdoor pedestrian thermal comfort during heatwave in Nagpur city. *Sustain. Cities Soc.* **2024**, *108*, 105450. [CrossRef]
53. Cai, Y.; Chen, Y.; Tong, C. Spatiotemporal evolution of urban green space and its impact on the urban thermal environment based on remote sensing data: A case study of Fuzhou City, China. *Urban For. Urban Green.* **2019**, *41*, 333–343. [CrossRef]
54. Du, J.; Xiang, X.; Zhao, B.; Zhou, H. Impact of urban expansion on land surface temperature in Fuzhou, China using Landsat imagery. *Sustain. Cities Soc.* **2020**, *61*, 102346. [CrossRef]
55. Sun, C.; Lian, W.; Liu, L.; Dong, Q.; Han, Y. The impact of street geometry on outdoor thermal comfort within three different urban forms in severe cold region of China. *Build. Environ.* **2022**, *222*, 109342. [CrossRef]
56. Miao, C.; Yu, S.; Hu, Y.; Zhang, H.; He, X.; Chen, W. Review of methods used to estimate the sky view factor in urban street canyons. *Build. Environ.* **2020**, *168*, 106497. [CrossRef]
57. *ISO 4354:2009*; Wind Actions on Structures. ISO: Geneva, Switzerland, 2009.
58. Ludwig, J.C.; Mortimor, S. *PHOENICSVR Reference Guide*; CHAM: London, UK, 2010.
59. Zheng, X.; Chen, L.; Yang, J. Simulation framework for early design guidance of urban streets to improve outdoor thermal comfort and building energy efficiency in summer. *Build. Environ.* **2023**, *228*, 109815. [CrossRef]
60. Aghamolaei, R.; Fallahpour, M.; Mirzaei, P.A. Tempo-spatial thermal comfort analysis of urban heat island with coupling of CFD and building energy simulation. *Energy Build.* **2021**, *251*, 111317. [CrossRef]
61. Bolot, R.; Imbert, M.; Coddet, C. On the use of a low-Reynolds extension to the Chen–Kim (k–ε) model to predict thermal exchanges in the case of an impinging plasma jet. *Int. J. Heat Mass Transf.* **2001**, *44*, 1095–1106. [CrossRef]
62. Radhi, H.; Sharples, S.; Assem, E. Impact of urban heat islands on the thermal comfort and cooling energy demand of artificial islands—A case study of AMWAJ Islands in Bahrain. *Sustain. Cities Soc.* **2015**, *19*, 310–318. [CrossRef]
63. Li, X.; Ma, Y.; Zhou, Q.; Zhang, X. Sparse large-scale high-order fuzzy cognitive maps guided by spearman correlation coefficient. *Appl. Soft Comput.* **2024**, *167*, 112253. [CrossRef]
64. Lin, H.J.; Ma, H.Y.; Zhang, M. Analysis of the variation characteristics of human thermal comfort in summer of China from 1980 to 2019 based on UTCI. *Adv. Clim. Change Res.* **2022**, *18*, 58.
65. Abdollahzadeh, N.; Biloria, N. Outdoor thermal comfort: Analyzing the impact of urban configurations on the thermal performance of street canyons in the humid subtropical climate of Sydney. *Front. Archit. Res.* **2021**, *10*, 394–409. [CrossRef]
66. Bröde, P.; Fiala, D.; Błażejczyk, K.; Holmér, I.; Jendritzky, G.; Kampmann, B.; Tinz, B.; Havenith, G. Deriving the operational procedure for the Universal Thermal Climate Index (UTCI). *Int. J. Biometeorol.* **2012**, *56*, 481–494. [CrossRef] [PubMed]
67. Zheng, L.; Lu, W. Urban micro-scale street thermal comfort prediction using a 'graph attention network'model. *Build. Environ.* **2024**, *262*, 111780. [CrossRef]
68. Turhan, C.; Özbey, M.F.; Çeter, A.E.; Akkurt, G.G. A Novel Data-Driven Model for the Effect of Mood State on Thermal Sensation. *Buildings* **2023**, *13*, 1662. [CrossRef]
69. Zhou, X.; Chen, H. Impact of urbanization-related land use land cover changes and urban morphology changes on the urban heat island phenomenon. *Sci. Total Environ.* **2018**, *635*, 1467–1476. [CrossRef] [PubMed]
70. Lin, H.; Hong, X.-C.; Wen, C.; Hu, F. The historical sensing of urban forest based on the indicators of CES and landscape categories: A case of Kushan scenic area in CHINA. *Ecol. Indic.* **2024**, *166*, 112440. [CrossRef]
71. Feng, L.; Wang, J.; Liu, B.; Hu, F.; Hong, X.; Wang, W. Does Urban Green Space Pattern Affect Green Space Noise Reduction? *Forests* **2024**, *15*, 1719. [CrossRef]
72. Ren, W.; Lu, P.; Wang, Y.; Hong, X.-C. Understanding the association between urban noise and nighttime light in China. *Sci. Rep.* **2024**, *14*, 31472. [CrossRef]
73. Lin, H.; Wen, H.; Zhang, D.-Y.; Yang, L.; Hong, X.-C.; Wen, C. How Social Media Data Mirror Spatio-Temporal Behavioral Patterns of Tourists in Urban Forests: A Case Study of Kushan Scenic Area in Fuzhou, China. *Forests* **2024**, *15*, 1016. [CrossRef]
74. Lin, H.; Wang, J.-B.; Zhang, X.; Hu, F.; Liu, J.; Hong, X.-C. Historical sensing: The spatial pattern of soundscape occurrences recorded in poems between the Tang and the Qing Dynasties amid urbanization. *Humanit. Soc. Sci. Commun.* **2024**, *11*, 730. [CrossRef]
75. Chinazzo, G.; Wienold, J.; Andersen, M. Daylight affects human thermal perception. *Sci. Rep.* **2019**, *9*, 13690. [CrossRef] [PubMed]
76. Yerlikaya-Özkurt, F.; Özbey, M.F.; Turhan, C. Modeling the mood state on thermal sensation with a data mining algorithm and testing the accuracy of mood state correction factor. *New Ideas Psychol.* **2025**, *76*, 101124. [CrossRef]
77. Turhan, C.; Özbey, M.F.; Lotfi, B.; Akkurt, G.G. Integration of psychological parameters into a thermal sensation prediction model for intelligent control of the HVAC systems. *Energy Build.* **2023**, *296*, 113404. [CrossRef]

78. Özbey, M.F.; Turhan, C. Investigating the Relationship Between Thermal Comfort and Human Psychology: A Review. *J. Build. Des. Environ.* **2024**, *3*, 5255.
79. Lin, T.P. Thermal perception, adaptation and attendance in a public square in hot and humid regions. *Build. Environ.* **2009**, *44*, 2017–2026. [CrossRef]

Disclaimer/Publisher's Note: The statements, opinions and data contained in all publications are solely those of the individual author(s) and contributor(s) and not of MDPI and/or the editor(s). MDPI and/or the editor(s) disclaim responsibility for any injury to people or property resulting from any ideas, methods, instructions or products referred to in the content.